CHAPTER 3

VARIATION OF SEMIVRIOGRAM MODELS WITH DIRECTION

When developing semivariogram models, it is often difficult to fit a model semivariogram to both the principle-axis and the minor-axes using traditional methods with anisotropy ratios. Currently a single model (possibly nested) is modified with anisotropy factors; these represent the relative range of the semivariogram for all three orthogonal axes. This technique is restrictive, and this discussion presents a method for relieving these restrictions by defining different semivariogram models, independently for each axis. These will be referred to as directional semivariograms. The process increases the kriging processing time by 80% to 200%, but the method offers the modeler greater flexibility, and simulations or estimations that are more representative of the site, because the spatial variation of the data can be more precisely defined.

3.1: Introduction

Semivariogram modeling is the foundation for much geostatistical analysis, and can also be the most difficult and time consuming portion of the analysis. In part, this is due to the computationally intensive calculations, but it is also due to the difficulty in defining semivariogram models which reasonably honor the experimental semivariograms in the principle and minor search directions. With the current techniques that use anisotropy factors (Englund and Sparks, 1988; Journel and Huijbregts, 1978; Deutsch and Journel, 1992), often it is not possible to model all the orthogonal experimental semivariograms exactly. Consequently compromises are required for the definition of one, or even all of the models. If the compromises are not too substantial, then this approach is acceptable, because, generally the kriged results are relatively insensitive to minor changes in the semivariogram. Though this insensitivity offers some comfort, it is not particularly satisfying.

This chapter describes a procedure, which allows the modeler to define a unique semivariogram model for each orthogonal axis of the experimental semivariogram. The algorithm uses components of each model to determine $\gamma(h)$ values between the axes. Anisotropy factors are not used; rather the modeler specifies the number of nests, sill and range components, and model

structure types independently for each axis. The only requirements are 1) the nugget must be the same for all models, and 2) the total sill must be the same at infinity. These two requirements are not particularly restrictive. Requiring the nugget to be the same is reasonable, because at zero distance, direction is irrelevant. The requirement that the total sill components are equal ensures that the kriging matrix is non-singular. If different sills are desired, then this requirement is met by defining an arbitrarily large range for the final nest to make up the balance of the sill component. The error induced by the final nest has no affect on the area of interest.

This technique allows the modeler to honor the results of the experimental semivariogram analysis, thus it is easier to model the data set and the results are more accurate. However, the calculation of $\gamma(h)$ is substantially more complex than traditional methods, therefore the method requires computational effort. The additional effort is comparable to the computational effort required for the search procedure and matrix solution portions of the kriging algorithm so, overall, the task is only increased by about 80% to 200% (based on observed differences in computation time for example data sets). This is acceptable, because the semivariogram model preparation is simplified, and the simulations or estimates should more closely honor the spatial statistics of the site.

3.2: Previous Work

Many techniques have been developed to estimate values of a variable at locations between sample points. These techniques are all based on the assumption that properties at unsampled locations are related to the properties at nearby points where samples have been taken. Some techniques are inaccurate due to assumptions related to the spatial variation and the relative importance of nearby data. For example, the inverse-distance method states that surrounding data (n = number of samples) have less importance with increased distance:

$$g_{i} = \frac{\sum_{i=1}^{n} \left(\frac{x_{i}}{d_{i}^{p}}\right)}{\sum_{i=1}^{n} \left(\frac{1}{d_{i}^{p}}\right)}$$
(3.1)

The rate (p) at which increasing distance (d) reduces the influence of a neighboring sample value (xi) is subject to debate. Various factors for p have been suggested; 1 (linear), 2, 1/x, based on the modelers previous experience with the technique, and its performance at similar sites. Consequently the results are subjective.

Kriging eliminates much of this subjectivity by utilizing the semivariogram as the spatial weighting function. The variance of the data and the rate of change in variance with direction and distance can be defined with the equation:

$$\gamma(h) = \frac{1}{2N} \sum_{i=1}^{N} (x_i - (x_i + h))^2$$
(3.2)

where $\gamma(h)$ describes spatial variance of all data pairs separated by a distance h. N is the number of pairs separated by the distance h, and x_i and x_i +h are the values at two points in the pair. Experimental semivariograms are complex, and for practical reasons are represented with one or more functions selected from a limited number of model types (e.g. spherical, exponential, Gaussian). These models are used because they guarantee the matrices in the kriging solution will be positive definite (i.e., the matrix is not singular). Even with these constraints, the semivariogram is a powerful mathematical tool for describing how a variable varies in space at a particular site.

Although semivariograms could be defined for an infinite number of directions, for practical reasons, variation is only defined along the principle orthogonal axes (X, Y, Z), creating an ellipsoid. As defined here, the X-axis is equivalent to the direction with the longest range (the principle axis), and the Y and Z-axes (orthogonal to X), have shorter, though not necessarily equal ranges. Although modeling and solving a more complicated system is theoretically possible, it would be extremely expensive computationally. To further simplify the solution, the semivariogram models for the Y and Z-axes have traditionally been described using anisotropy factors related to the X-axis. This simplification is used extensively in current kriging models (Deutsch and Journel, 1992; Gómez-Hernández and Srivastava, 1990), because it is computationally efficient, however it compromises accuracy and requires more time of the modeler when the same semivariogram model does not fit the experimental semivariogram in all directions. The technique presented here allows the modeler to specify unique semivariogram models for each axis.

3.3: Theory

Two steps of the kriging process are modified to incorporate directional semivariograms into the kriging algorithm: 1) the search for nearest neighbors, and 2) the calculation of the covariance components of the kriging matrix.

The first step in estimating the value for a grid location is to find the influential neighboring points. For isotropic situations the closest sample points are the best estimators. For anisotropic situations, the best estimators are those points with the smallest spatial variance calculated from the model semivariogram (γ (h)). Using anisotropy factors, the sample point locations are transformed to equivalent isotropic space, using a simple transformation and rotation, based on the orientation of the principle model axis, and the anisotropy factors of the minor-axes. Once transformed, the estimation variance is solely a function of the distance between the grid location and the sample point, therefore γ (h) doesn't have to be calculated. Conventional techniques (Deutsch and Journel, 1992; Gómez-Hernández and Srivastava, 1990), use Pythagoras' Theorem to find the closest points. When directional semivariogram models are used, direction as well as distance is important. When

different model equations, sills, and structures are used for the orthogonal axes, a simple transformation and rotation is not possible, because the magnitude of $\gamma(h)$ is not solely related to distance (Figure 3.1). For this reason, $\gamma(h)$ must be calculated for each sample in the search

a). Major Semivariogram Model Axis 0.4 0.3 gamma (h) Model Parameters Range Model 0.1 0.05 450 Spherical 200 0.2 0.022 Spherical 0.0 100 200 300 400 500 distance (m)

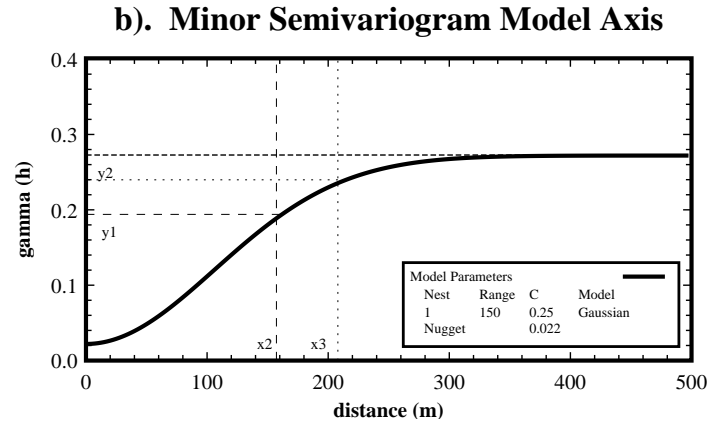


FIGURE 3-1. When directional semivariograms are used, distance alone does not determine the most influential neighboring points. In this example, all points in the minor model axis direction (b) that are separated by less than x_2 (158 m) have smaller γ (h)'s than points separated by x_1 (109 m) on the major-axis (a). The same is true for x_3 and x_2 respectively.

neighborhood, and those points with the smallest $\gamma(h)$ values are the best estimators.

Once the most influential neighboring data points have been selected, the kriging matrix is solved as usual, with the exception of the $\gamma(h)$ calculation. Again, for directional semivariograms, it is not possible to transform points into isotropic space, therefore component of the individual axes must be resolved. Whether $\gamma(h)$ is being calculated to determine the most influential neighbors or

individual components of the kriging matrix, the same technique is used as described in the following section.

3.3.1 Equation and Proof

Calculating $\gamma(h)$ to determine the nearest neighbors for a grid location, or to define individual components of the kriging matrix, requires the equation for an ellipsoid:

$$\frac{x^2}{a^2} + \frac{y^2}{b^2} + \frac{z^2}{c^2} = 1 \tag{3.3}$$

Using this equation, it is possible to separate the components of each semivariogram model for any vector (Figure 3.2). One point is translated to the axis origin, and the second point is positioned at |x|, |y|, and |z|, along the separation vector (h). Here a, b, and c, represent the maximum practical ranges of the semivariograms model along the X-, Y-, and Z-axes respectively. In this section only, when the actual ranges are used the a_{actual} , b_{actual} , and c_{actual} , subscripts will be used. The practical range refers to the distance where the semivariogram model meets the variance. For the Exponential and Gaussian models, this is defined as 95% of the variance. The practical ranges for different models are defined (Journel and Huijbregts, 1978):

Model Type	Practical Range
Spherical	range
Exponential	3 x range
Gaussian	sqrt(3) x range
Linear	range

If the unadjusted range and not the practical range is used, the axis defined with the model using the longest practical range will be under-weighted. The equations for determining each component $\gamma(h)_{X,Y,Z}$ and the resultant $\gamma(h)$ are derived below. The components of each axis for each structure of the nested semivariogram model can be related through the aspect factors:

$$f = a/b \tag{3.4a}$$

$$g = a/c (3.4b)$$

$$p = b/c (3.4c)$$

Rearranging Equation 3.3, the ellipsoid factors a², b², and c² for the search vector are solved:

$$\frac{x^2}{a^2} + \frac{f^2y^2}{a^2} + \frac{g^2z^2}{a^2} = 1$$

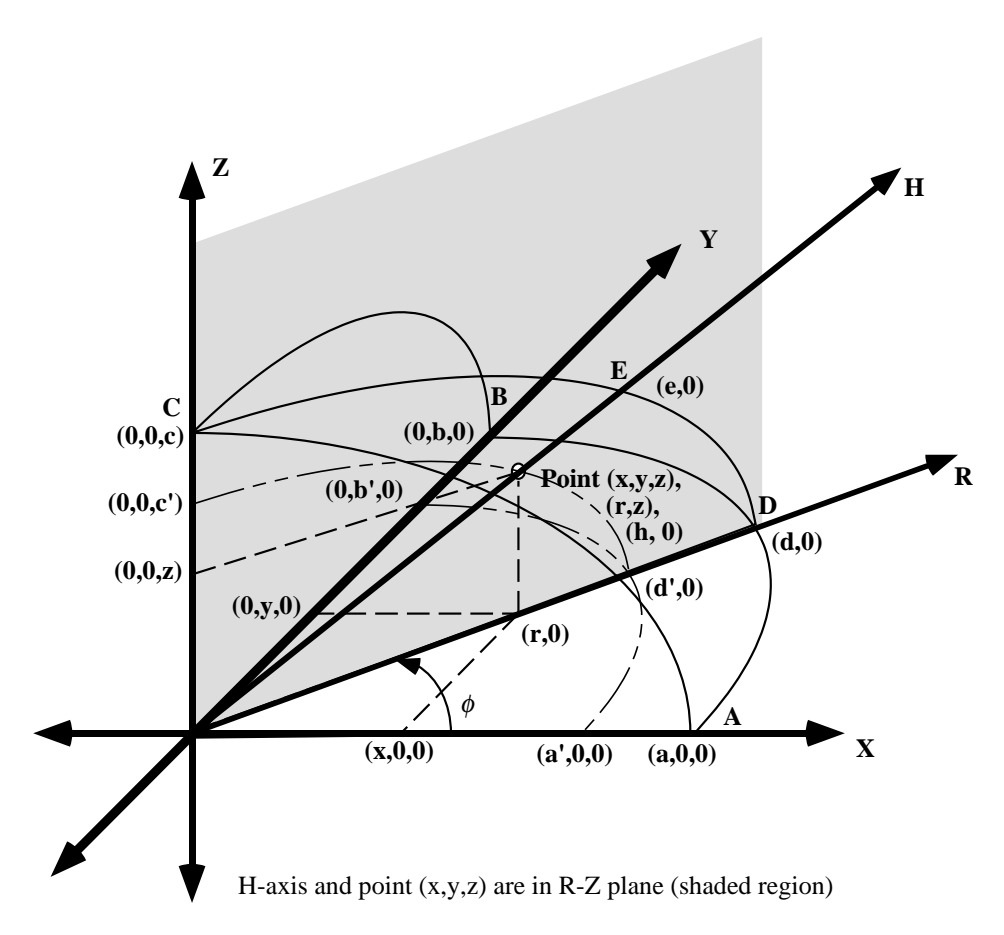


FIGURE 3-2. Directional semivariogram analysis components.

$$a^{2} = x^{2} + f^{2}y^{2} + g^{2}z^{2}$$

$$\frac{x^{2}}{f^{2}b^{2}} + \frac{y^{2}}{b^{2}} + \frac{p^{2}z^{2}}{b^{2}} = 1$$
(3.5a)

$$b^{2} = \frac{x^{2}}{f^{2}} + y^{2} + p^{2}z^{2}$$
(3.5b)

$$\frac{x^2}{g^2c^2} + \frac{y^2}{p^2c^2} + \frac{z^2}{c^2} = 1$$

$$c^{2} = \frac{x^{2}}{g^{2}} + \frac{y^{2}}{p^{2}} + z^{2}$$
(3.5c)

Where a', b', and c' represent the X, Y, and Z-axis intercepts for an ellipsoid passing through an arbitrary point, (x, y, z) along the same vector, where the aspect rations defined by a, b, and c remain true, the following relationships are also true:

$$\frac{a'}{b'} = \frac{a}{b} = f \tag{3.5d}$$

$$\frac{b'}{c'} = \frac{b}{c} = p \tag{3.5e}$$

$$\frac{a'}{c'} = \frac{a}{c} = g \tag{3.5f}$$

An additional axis, R, is also required. R is defined by the intersection of the X-Y plane, and the vertical plane passing through the point (x, y, z). To determine the semivariogram components, the point r, which lies on the R-axis, vertically below the point (x, y, z) is defined:

$$r^2 = x^2 + y^2 (3.5g)$$

Two additional points of interest are where the semivariogram model ellipsoid and the ellipsoid passing through (x, y, z) cross the R-axis; these are d and d' respectively. Defining these two ellipsoids, with the aspect ratios described above, the components of each semivariogram model can be derived. One new aspect ratio is needed between the R- and Z-axes.

$$q = d/c (3.6)$$

The distances a, b, c, and d represent the practical model range and a', b', c', and d' represent the practical component range along each axis for the point (x, y, z). The parameter d represents the semivariogram model along the R-axis and is a combination of models a and b. Once a, b, x, and y are known, then d can be determined. For a circle, the angle f is described as:

$$\phi = \tan^{-1} \left(\frac{y}{x} \right) \tag{3.7}$$

Usually, the model semivariogram ellipse (X-Y plane) will not be a circle, therefore the anisotropy must be removed to determine the component angle f. This is the product of y and the aspect ratio of the ellipse (f in the X-Y plane, major/minor dimension):

$$\phi = \tan^{-1} \left(\frac{yf}{x} \right) \tag{3.8}$$

The components of a and b can then be described by dividing $(90^{\circ} - f)$ by 90° , and multiplying by b and a, plus a:

$$a_{\phi \text{ comp}} = \frac{90^{\circ} - \phi}{90^{\circ}} a \tag{3.9}$$

$$b_{\phi \text{ comp}} = \frac{\phi}{90^{\circ}} b \tag{3.10}$$

The components can then be summed to calculate d':

$$\begin{split} d &= a_{\phi \; comp} + b_{\phi \; comp} \\ d &= \frac{90^{\circ} - \phi}{90^{\circ}} a + \frac{\phi}{90^{\circ}} b \\ d &= a + \frac{\phi}{90^{\circ}} b - \frac{\phi}{90^{\circ}} b \\ d &= \frac{\phi}{90^{\circ}} (b - a) + a \end{split} \tag{3.11}$$

By expanding f and solving, using radians, the equation may be rewritten:

$$d = \frac{\tan^{-1}\left(\frac{yf}{x}\right)}{\frac{\pi}{2}}(b-a) + a$$
(3.12)

d' can be determined by proportion:

$$d'=d\frac{a}{a'}=d\frac{b}{b'}$$
(3.13)

Given distances a', b', c', and d', it is possible to solve directly for $\gamma(a')$, $\gamma(b')$, and $\gamma(c')$. To solve for $g(d'_{actual})$, the argument is used for d is repeated, The components of $\gamma(a'_{actual})$ and $\gamma(b'_{actual})$ can

then be described by dividing (90° - f) by 90°, and multiplying by $\gamma(b'_{actual})$ and $\gamma(a'_{actual})$, plus $\gamma(a'_{actual})$:

$$\gamma(a'_{actual})_{\phi comp} = \frac{90^{\circ} - \phi}{90^{\circ}} \gamma(a'_{actual})$$
(3.14)

$$\gamma(b'_{\text{actual}})_{\phi \text{ comp}} = \frac{\phi}{90^{\circ}} \gamma(b'_{\text{actual}})$$
(3.15)

The components can then be summed to calculate $\gamma(d'_{actual})$:

$$\begin{split} \gamma(d'_{actual}) &= \gamma(a'_{actual})_{\phi \ comp} + \gamma(b'_{actual})_{\phi \ comp} \\ \gamma(d'_{actual}) &= \frac{90^{\circ} - \phi}{90^{\circ}} \gamma(a'_{actual}) + \frac{\phi}{90^{\circ}} \gamma(b'_{actual}) \\ \gamma(d'_{actual}) &= \gamma(a'_{actual}) + \frac{\phi}{90^{\circ}} \gamma(b'_{actual}) - \frac{\phi}{90^{\circ}} \gamma(a'_{actual}) \\ \gamma(d'_{actual}) &= \frac{\phi}{90^{\circ}} (\gamma(b'_{actual}) - \gamma(a'_{actual})) + \gamma(a'_{actual}) \end{split}$$

$$(3.16)$$

By expanding f and solving, the equation may be rewritten:

$$\gamma(d'_{actual}) = \frac{\tan^{-1}\left(\frac{yf}{x}\right)}{\frac{\pi}{2}} \left(\gamma(b'_{actual}) - \gamma(a'_{actual})\right) + \gamma(a'_{actual})$$
(3.17)

To solve for $\gamma(e'_{actual})$, where e' is the distance from the origin to the point (x, y, z), steps similar to those used to generate d and $\gamma(d'_{actual})$ are required. Allowing $\gamma(d'_{actual})$ to be equivalent to $\gamma(a'_{actual})$, and $\gamma(c'_{actual})$ equivalent to $\gamma(b'_{actual})$, this yields:

$$\gamma(e'_{actual}) = \frac{\tan^{-1}\left(\frac{zq}{r}\right)}{\frac{\pi}{2}} \left(\gamma(c'_{actual}) - \gamma(d'_{actual})\right) + \gamma(d'_{actual})$$
(3.18)

These calculation must be evaluated for each nest of the model structure except the nugget $(\gamma(h)_0)$. The nugget, having zero distance, by definition is the same for all axes. This also implies that the number of structures in every direction must be equal. This restriction can be negated by giving undesired nests a zero variance component and the same range as the previous structure. The final $\gamma(e'_{actual})$ estimate is the summation on the nugget and the nested structure components:

$$\gamma(e'_{actual}) = \sum_{i=0}^{s} \gamma(e'_{actual})_i$$
; where $s = number of structures$
(3.19)

3.3.2: Positive Definite Matrix Issues

The models selected for the semivariogram, must yield a positive definite kriging matrix (Journel and Huijbregts, 1978). If the matrix is not positive definite, there may be no solution or there may be several different solutions (Isaaks and Srivastava, 1989), and the kriging variance may be negative (Journel and Huijbregts, 1978). The various model types used here (spherical, exponential, Gaussian, and logarithmic) have proven to be positive definite both individually and in combination as nested structures (Journel and Huijbregts, 1978). Although the equations are merged in a different manner for directional semivariograms than for traditional kriging, it is assumed that the matrix remains positive definite. In practice, several indicators used to determine whether the matrix is not positive definite, are 1) matrices that are singular, 2) have large positive or negative kriging weights (much larger or smaller then \pm 1.0), and 3) the occurrence of negative estimation variances. Proving that the equations are positive definite is a difficult task (Christakos, 1984; Isaaks and Srivastava, 1989), but in summary, for a symmetric (n x n) matrix to be positive definite, it must satisfy any one of the following conditions (Burden and Faires, 1985; Isaaks and Srivastava, 1989; Strang, 1988):

- i) $x^tAx > 0$ for all non-zero vectors x.
- ii) All the eigenvalues (λ_i) of A are greater than 0.
- iii) All the upper left submatrices A_k have positive determinants.
- iv) All the pivots (d_i, without row exchange) are greater than 0.

for every n-dimensional column vector $\mathbf{x} \neq 0$, where A is the kriging matrix, \mathbf{A}_k is a submatrix of A, x is any vector (appropriately dimensioned), and \mathbf{x}^t is the transpose of x.

3.3.2.1: Problems With the Positive Definite Assumption

Some problems with large positive and negative weights and negative kriging variances were encountered when Gaussian models were used with the directional kriging method. Many of the problematic matrices were confirmed to be positive definite based on tests i) and ii). The problems were attributed to the unstable nature of the Gaussian model with small nuggets (Ababou, Bagtzoglou, et al., 1994; Posa, 1989). Ababou, et al (1994), state that this is a common problem, particularly with Gaussian models that have small nugget values. The kriging matrix becomes more unstable and approaches singularity at small h values. This tendency can be estimated using the kriging matrix (A) conditioning number $\kappa(A)$:

 $\kappa(A) = |MAX \text{ eigenvalue}| / |MIN \text{ eigenvalue}|$

The Gaussian model, is one of the most problematic (2 to 14 times worse than hole-exponential models (which are one of the best) (Ababou, et al., 1994)) and most unstable, and tends to have minimum eigenvalues near 0.0. Also, because the model is relatively flat at small h values (unlike all other models), the problem prevails at larger h values than for other models (Posa, 1989). Because of this instability, it is sometimes better to select a model which does not physically fit the data as well as another model, but is more robust (Posa, 1989).

3.4: Modification of Algorithms

In this project, the GSLIB ktb3dm (Deutsch and Journel, 1992), and SISIM3D (Gómez-Hernández and Srivastava, 1990; McKenna, 1994) algorithms were modified to build the kriging matrix using both anisotropic semivariogram models and directional semivariogram models.

3.4.1: Algorithm Constraints

Although directional semivariogram models relax many of the constraints in defining spatial variation, there are several limitations. Some of these limitations arise from the theory, and some from the implementation. The limitations are:

- The number of semivariogram models for each axis must be equal. This is a minor limitation, because extra models can be added as needed with a zero variance component, and a range equal to the final desired range. If this is not done, there may be ambiguity in how the semivariogram models are evaluated.
- The sill for all axes must be equal. Again this is a minor limitation. If the variance in one direction is smaller than another in the grid area, the remaining variance component may be added to the final nest, while the range for the final nest is set to a range much greater than the size of the simulated area (or the search distance for that matter). This constraint is required to ensure positive definite matrix solutions.
- Gaussian models may be used with small or zero nugget values, but the modeler must be aware that the results can be unstable. The algorithm presented here tests for large (±) weights and warns the modeler. The algorithm can remove data points (the point associated with the largest absolute kriging weight) from the kriging matrix until the results stabilize, or until there are too few points to estimate the grid location, however estimates resulting from such elimination should be considered highly suspect (See Rocky Mountain Arsenal example described below), and one may wish to compromise and use a larger nugget (often the problem with Gaussian models), or a different model type all together.

3.4.2: Computational Cost

Although use of directional semivariograms is computationally intensive, the increased computation, is significant, but not excessive. In several test cases, the computation time increased between 80% and 200%. The increased computation occurs mainly in the search algorithm that identifies the most influential neighbors for each grid location and in the additional overhead for calculating each covariance value of the kriging matrix.

The search algorithm in the traditional technique includes two main steps: 1) transformation of the sample data to isotropic space, and 2) calculation of the distance between each point and each grid location being estimated. In addition to these steps, the directional semivariogram technique requires that $\gamma(h)$ be calculated for each sample point, relative to the position of the grid position being estimated. To determine the neighboring points with the smallest spatial variances, traditional techniques calculate only the relative distance between sample points in isotropic space, and the point being estimated. This is adequate, because the spatial variance is only a function of distance. When using directional semivariogram models, transformed isotropic distances are not sufficient to rank sample points; direction is also important, thus $\gamma(h)$ for the separation between each sample and the grid location must be ranked. Calculating $\gamma(h)$ in the search phase, adds most of the increased computational effort.

The calculation of $\gamma(h)$ for the kriging matrix also requires additional effort. Although this step is generally less expensive in computation time than the search step because it is applied only to the selected nearest neighbor points and not to all points within the search neighborhood.

To solve the kriging problem, the kriging matrix must also be solved using either Gauss elimination or a more efficient LU decomposition (Alabert, 1987). These calculations are unaffected by the method used to define the semivariogram models, but because this is a computationally intensive task, the increased cost due to directional semivariogram modeling is less severe.

3.5: Examples

Several example models and data sets are used to demonstrate the applicability and validity of using directional semivariogram models.

3.5.1: Comparison With the Classic Method

In addition to the mathematical proof above, it is also important to demonstrate that the algorithm and the software are correct. Two approaches are pursued to evaluate the algorithm. First, conditions modeled using anisotropy factors with traditional methods are duplicated using directional semivariogram models that mimic the anisotropy factors. Then, model results using directional semivariogram models, that cannot be described with anisotropy factors, are compared with manual calculations.

3.5.1.1: Anisotropic Case: Directional Components Equivalent to Anisotropy Factors

To demonstrate that the directional semivariogram model technique produces the same results as the conventional technique using anisotropy factors, a small synthetic data set with eleven data points was created (Figure 3.3a). Given equivalent model input, the results are identical. The semivariogram models for each case are:The principal axis is oriented to the Northwest. The map

Method	Axis	Model Type	Ramge	Sill	Nugget	Y-Anisotropy
Anisotropic	All	Spherical	100	0.14	0.02	0.4
		Spherical	250	0.11		0.75
Directional	X	Spherical	100	0.14	0.02	NA
		Spherical	250	0.11		NA
	Y	Spherical	40	0.14	0.02	NA
		Spherical	187.5	0.11		NA

in Figure 3.3b is the traditional simple kriged map using a single semivariogram model with anisotropy factors. Figure 3.3c was produced using directional semivariograms. When the two maps are subtracted from one another, the difference is zero at every grid location, indicating that the directional semivariogram method is able to correctly reproduce the simple case where anisotropic conditions exist and the perpendicular semivariogram models are related by anisotropy factors.

3.5.1.2: Anisotropic Case - Manual Solution

To demonstrate that the method produces the answers we intuitively expect, several g(h) values are calculated manually for several points at various orientations with one model set (three orthogonal directional semivariogram models). A second calculation will be made for the multi-nested model defined in Figure 3.1. The first model set is defined as:

Axis	Model Type	Range	Sill	Nugget
X	Spherical	125	5	1
Y	Gaussian	75	5	1
Z	Spherical	30	5	1

for the points:

Sample	X	Y	Z
I	87	0	0
II	43	26	0
III	43	26	-11

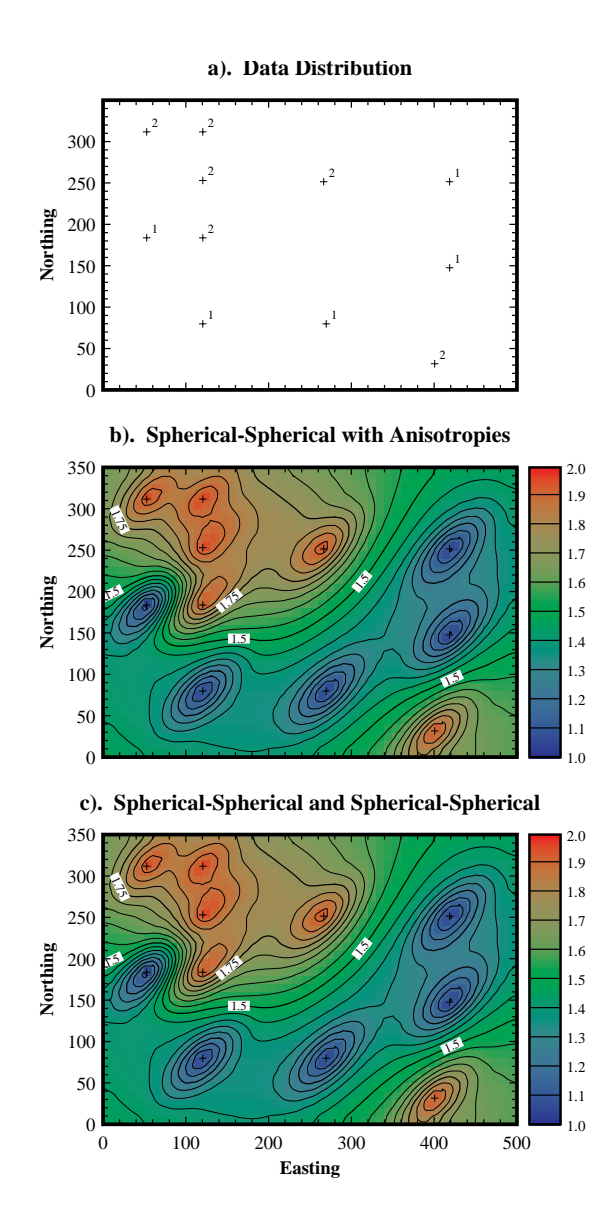


FIGURE 3-3. Example results confirming directional semivariograms can exactly mimic anisotropy factors: a) sample data set, b) SK map using anisotropic factors, c) SK map using directional semivariograms.

the solutions are calculated:

I). For the point (87, 0, 0), the solution is simple. The point lies along a principal axis, and in this case has a zero Y and Z component. $\gamma(h)$ can therefore be calculated directly, using the standard spherical equation for the X direction:

$$\gamma(h) = \sum_{i=0}^{s} C_i$$
; where $s =$ number of structures (3.19)

$$\gamma(h)_{1} = C_{1} \left[1.5 \frac{h}{r} - 0.5 \frac{h^{3}}{r^{3}} \right]$$
(3.20)

$$\gamma(h)_1 = 5 \left[1.5 \frac{87}{125} - 0.5 \frac{87^3}{125^3} \right] = 4.377$$

$$\gamma(h)_0 = \text{nugget} = 1.0$$

$$\gamma(h) = \gamma(h)_1 + \gamma(h)_0 = 4.377 + 1.0 = 5.377$$

where h is the separation distance, and r is the model range (for this equation only).

II). For the point (43, 26, 0), the first step is to define the nugget; $\gamma(h)_0 = 1.0$. Next the X and Y directional components must be calculated (the Z axis has a zero component). The X and Y intercepts of the ellipse that passes through (43, 26) and has an X/Y aspect ratio of 125/75 (a/b) (remember the actual Gaussain range must be multiplied by the to determine the practical ellipsoid range). The intercepts, a' and b' are determined using the standard equation for an ellipse (Equation 3.3):

$$a^2 = (43)^2 + \left(\frac{125}{75\sqrt{3}}\right)^2 (26)^2$$
 (using Equation 3.5a)

a' = 49.74

$$b^{2} = \frac{(43)^{2}}{\left(\frac{125}{75\sqrt{3}}\right)^{2}} + (26)^{2}$$

(using Equation 3.5b)

$$b' = 50.97$$

Given the X and Y intercepts, $\gamma(h)$ for each ellipsoid axis is calculated:

$$\gamma_{x}(h)_{1} = 5 \left[1.5 \frac{49.74}{125} - 0.5 \frac{49.74^{3}}{125^{3}} \right] = 2.827$$

$$\gamma_{y}(h)_{1} = C_{1} \left(1 - e^{-(h)^{2}/(r)^{2}} \right)$$

$$\gamma_{y}(h)_{1} = 5 \left(1 - e^{-(50.97)^{2}/(75)^{2}} \right) = 1.849$$
(3.21)

Note that the actual and not practical range is used to calculate $\gamma_y(h)_1$. Once the maximum contributions for each axis have been determined, the component contribution of each must be determined. This is done by determining the effective angle of the vector (43, 26) in the X-Y plane. The effective angle is:

$$\phi = \tan^{-1} \left(\frac{26 \frac{125}{75 \sqrt{3}}}{43} \right) = 30.19^{\circ}$$

Given this angle, the components of $\gamma_x(h)$ and $\gamma_y(h)$ can be determined. Intuitively the X-axis component can be defined as:

$$2.827 \frac{(90^{\circ} - 30.19^{\circ})}{90^{\circ}} = 1.879$$

and the Y-axis component is:

$$1.849 \left(\frac{30.19^{\circ}}{90^{\circ}} \right) = 0.620$$

Adding the two components together yields a directional $\gamma(h)$ of 2.499. This yields the same result as if Equation 3.18 were used:

$$\gamma_{d} \cdot (h)_{1} = \frac{\tan^{-1} \left(\frac{26 \frac{125}{75\sqrt{3}}}{43} \right)}{\frac{\pi}{2}} (1.849 - 2.827) + 2.827 = 2.449$$

When the $\gamma(h)_i$ components are summed, the total estimate for $\gamma(h)$ is 2.449+1.0 which equals 3.449.

III). The same approach may be used for the last point (43, 26, -11), $\gamma(h)_0 = 1.0$, and the X, Y, and Z directional components must be calculated. The first step is to calculate the X, Y, and Z intercepts for the ellipsoid that passes through (43, 26, -11) and has an X/Y aspect ratio of 125/75, a X/Z aspect ratio of 125/30, and a Y/Z aspect ratio of 75/30. The intercepts, a', b', and c' are determined using the standard equation for an ellipsoid (Equation 3.3):

$$a^{2} = (43)^{2} + \left(\frac{125}{75\sqrt{3}}\right)^{2} (26)^{2} + \left(\frac{125}{30}\right)^{2} (-11)^{2}$$
 (using Equation 3.5a)

a' = 67.64

$$b^{2} = \frac{(43)^{2}}{\left(\frac{125}{75\sqrt{3}}\right)^{2}} + (26)^{2} + \left(\frac{75\sqrt{3}}{30}\right)^{2} (-11)^{2}$$

(using Equation 3.5b)

b' = 70.29

$$c^{2} = \frac{(43)^{2}}{\left(\frac{125}{30}\right)^{2}} + \frac{(26)^{2}}{\left(\frac{75\sqrt{3}}{30}\right)^{2}} + (-11)^{2}$$

(using Equation 3.5c)

$$c' = 16.23$$

Given the X, Y, and Z intercepts, $\gamma(h)_1$ for each ellipsoid axis is calculated:

$$\gamma_x(h)_1 = 5 \left[1.5 \frac{67.64}{125} - 0.5 \frac{67.64^3}{125^3} \right] = 3.662$$

$$\gamma_y(h)_1 = 5\left(1 - e^{-(70.29)^2/(75)^2}\right) = 2.923$$

$$\gamma_z(h)_1 = 5 \left[1.5 \frac{16.23}{30} - 0.5 \frac{16.23^3}{30^3} \right] = 3.662$$

Using the same methods as described for point II, $\gamma_{d'}(h)_1$ can be determined:

$$\gamma_{d'}(h)_{1} = \frac{\tan^{-1}\left(\frac{26\frac{125}{75\sqrt{3}}}{43}\right)}{\frac{\pi}{2}}(2.923 - 3.662) + 3.662 = 3.414$$

Now that the X-Y axis contributions have been merged, the Z-axis component is incorporated. This requires that d' and r be calculated. d' is calculated by merging equations 3.12 and 3.13:

$$d' = \frac{\tan^{-1}\left(\frac{yf}{x}\right)}{\frac{\pi}{2}}(b'-a') + a'$$

$$d' = \frac{\tan^{-1}\left(26\frac{125}{75\sqrt{3}}\right)}{\frac{\pi}{2}}(70.29 - 67.64) + 67.64 = 68.53$$

$$r = \sqrt{(43)^2 + (26)^2} = 50.25$$

Similar steps are used in the vertical R-Z plane through (43, 26, -11) as were undertaken in the X-Y plane,. For purposes of calculating the vector length h, only absolute values for each coordinate are used, and c' and d' are substituted for c and d. The angle f from R to Z is:

$$\phi = \tan^{-1} \left(\frac{11 \frac{68.53}{16.23}}{50.25} \right) = 42.75^{\circ}$$

Given this angle, the components of $\gamma_d(h)_1$ and $\gamma_z(h)_1$ can be determined.

$$3.414 \frac{(90^{\circ} - 42.75^{\circ})}{90^{\circ}} = 1.792$$

and the Z-axis component is:

$$3.662 \frac{42.75^{\circ}}{90^{\circ}} = 1.739$$

Adding the two components together yields a directional $\gamma(h)_1$ of 3.531. This yields the same result as if Equation 3.23 were used:

When the $\gamma(h)_i$ components are summed, the total estimate for $\gamma(h)$ is 3.531 + 1.0 which equals 4.531.

For the final example, the one and two-nested structure models shown if Figure 3.1 are used. This example demonstrates that the modeler is not required to specify the same number of model structures in all directions. Although the algorithm requires the number of structures to be equal, the algorithm can internally add extra structures as needed without affecting the model description. The calculations will be made for two points separated by 200m at a 45° angle (x = 141.1, y = 141.1). The models are defined:

Direction	Range	C	Model	Nest
North-South	450	0.05	Spherical	2
	200	0.20	Spherical	1
		0.022	Nugget	0

Direction	Range	C	Model	Nest
East-West	150	0.00	Gaussian	2
	150	0.25	Gaussian	1
		0.22	Nugget	0

Note that the number of structures are the same in both directions, but the East-West models second nest has a zero sill (C) component. As described in the earlier examples, the nugget is a constant with direction, therefore $\gamma(h)_0 = 0.022$. The remaining $\gamma(h)_i$ values are calculated as follows (geometric interpretations are shown in Figure 3.4):

$$a_{1}^{2} = (141.4)^{2} + \left(\frac{150\sqrt{3}}{200}\right)^{2} (141.4)^{2}$$

$$a_{1}^{2} = 231.9$$

$$b_{1}^{2} = \frac{(141.4)^{2}}{\left(\frac{150\sqrt{3}}{200}\right)^{2}} + (141.4)^{2}$$

$$b_{1}^{2} = 178.4$$

$$\gamma_{x}(h)_{1} = 0.25 \left(1 - e^{-\left(150\sqrt{3}\right)^{2}/(231.9)^{2}}\right) = 0.1789$$

$$\gamma_{y}(h)_{1} = 0.20 \left[1.5 \frac{200}{178.4} - 0.5 \frac{200^{3}}{178.4^{3}}\right] = 0.1954$$

$$\tan^{-1}\left(\frac{141.4 \frac{150\sqrt{3}}{200}}{141.4}\right)$$

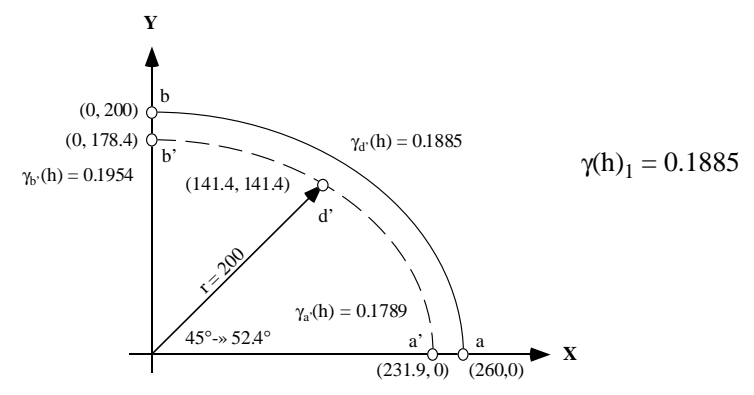
$$\gamma_{d} \cdot (h)_{1} = \frac{\pi}{(0.1954 - 0.1789) + 0.1789} = 0.1885$$

For the second nest, there is no East-West component. For the algorithm to work correctly, an additional East-West structure must be defined (the number of structures for all axes must be equal). To satisfy the algorithm and the specified Gaussian model, a zero sill component is used, and the range is set equal to the previous nest. This manipulation satisfies the algorithm, and leaves the model definition unchanged:

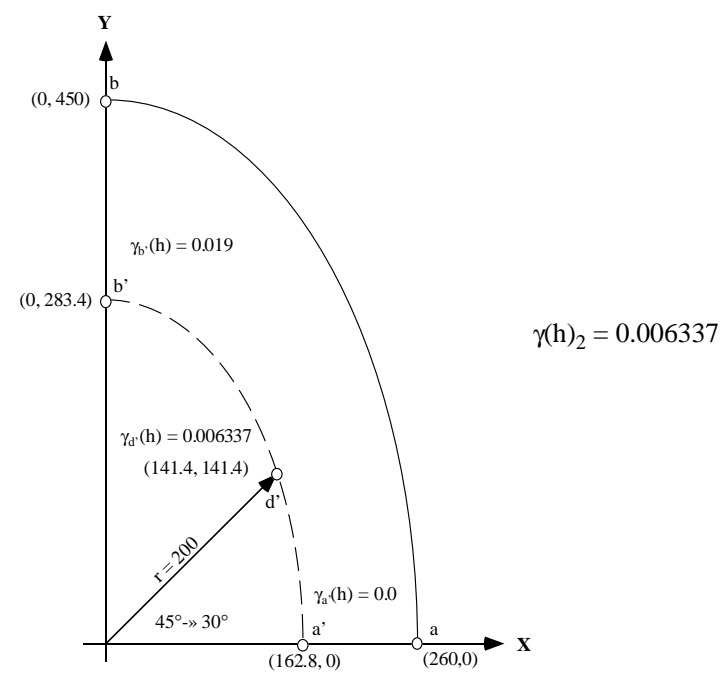
STEP 1: Determine Nugget

 $\gamma(h)_0 = 0.022$

STEP 2: Determine C_1 Geometry (Nest 1)



STEP 3: Determine C₂ Geometry (Nest 2)



STEP 4: Sum Components

 $\gamma(h) = 0.2168$

FIGURE 3-4. Geometric steps for calculating directional semivariogram model defined in Figure 3.1. The major axis is aligned North-South, and the minor axis is aligned East-West. Note, the 45° angle is transformed (-») based on the anisotropy of the ellipsoid.

$$a_{2}^{2} = (141.4)^{2} + \left(\frac{150\sqrt{3}}{450}\right)^{2} (141.4)^{2}$$

$$a_{1}^{2} = 162.8$$

$$b_{2}^{2} = \frac{(141.4)^{2}}{\left(\frac{150\sqrt{3}}{450}\right)^{2}} + (141.4)^{2}$$

$$b_{1}^{2} = 283.4$$

$$\gamma_{x}(h)_{2} = 0.00 \left(1 - e^{-\left(150\sqrt{3}\right)^{2} / (162.8)^{2}}\right) = 0.0000$$

$$\gamma_{y}(h)_{2} = 0.05 \left[1.5 \frac{450}{283.4} - 0.5 \frac{450^{3}}{283.4^{3}}\right] = 0.01900$$

$$\tan^{-1} \left(\frac{141.4 \frac{150\sqrt{3}}{450}}{141.4}\right)$$

$$\gamma_{d}(h)_{2} = \frac{\pi}{2}$$

$$(0.1900 - 0.0000) + 0.0000 = 0.006337$$

The final step is to sum the $\gamma_{d'}(h)_i$ components:

$$\gamma(h) = \sum_{i=0}^{2} \gamma_{d} \cdot (h)_{i} = \gamma_{d} \cdot (h)_{0} + \gamma_{d} \cdot (h)_{1} + \gamma_{d} \cdot (h)_{2}$$
$$= 0.022 + 0.1885 + 0.006337$$
$$= 0.2168$$

3.5.2: Practical Applications

A synthetic and a field data set are used to demonstrate the effectiveness and usefulness of the technique. For the synthetic case, the same data set that was used in section 3.4.1.1 is utilized, though different assumptions about the X and Y semivariogram models are made. The field data set is residual bedrock elevation data from the Rocky Mountain Arsenal, Commerce City, Colorado.

3.5.2.1: Synthetic Directional Semivariogram Demonstration Set

To demonstrate that directional semivariogram models can have a significant impact on model results, the data set in Figure 3.3a is used, but in this case anisotropy factors are not used, rather directional semivariogram models are defined. Since this is a synthetic data set, none of the following models can be argued to be the best representation of site conditions, any more than the other models, but the exercise demonstrates that directional semivariograms offer great flexibility in adjusting the estimations to match perceived or measured site conditions. Three different site scenarios were calculated based on the following directional semivariogram models (Figure 3.5):

Scenarios	Axis	Nest	Model Type	Range	Sill	Nugget
I	X	1	Spherical	100	0.14	0.02
		2	Spherical	250	0.11	
	Y	1	Gaussian	23.1	0.14	0.02
		2	Exponential	62.5	0.11	
II	X	1	Spherical	100	0.14	0.02
		2	Spherical	250	0.11	
	Y	1	Gaussian	23.1	0.07	0.02
		2	Exponential	62.5	0.18	
III	X	1	Spherical	100	0.14	0.02
		2	Spherical	250	0.11	
	Y	1	Gaussian	62.5	0.25	0.02

The ranges of the exponential and Gaussian models are significantly different from the spherical model ranges used for the Y-axis (40m and 187.5m for two nests) in Section 3.4.1.1. The range of a exponential and Gaussian model must be multiplied by the following factors to yield the equivalent spherical range (Deutsch and Journel, 1992):

Model Tyoe	Practical Range (a)
Exponential	3a
Gaussian	a(sqrt(3))

Despite these rules of thumb, the range for the scenario III Gaussian model was set to 1/3 of the two-nested Spherical model's range. This configuration more closely resembles the original and alternate Y-axis models (Figure 3.5, the climbing limbs of the models are more similar, even if the full Gaussian range is somewhat reduced). These models, are oriented with their major axes to the Northeast. In Figure 3.6a, the structures for the minor axis were substituted with Gaussian and Exponential models. In Figure 3.6b, the sill terms for the first structure in the minor axis (Y) was lowered to 0.7, and the sill for the second structure was raised to 0.18. Finally, in Figure 3.6c, the minor axis was substituted with a single Gaussian model (sill = 0.25, a second structure with a 0.0 sill component is assumed by the algorithm). The estimations (Figure 3.3a,b, and Figure 3.6a-c) show the same general NE-SW trend, but vary in detail. The differences are easiest to see near the

Semivariogram Models

Semivariogram Ellipse Minor-Axis: Various Test Cases

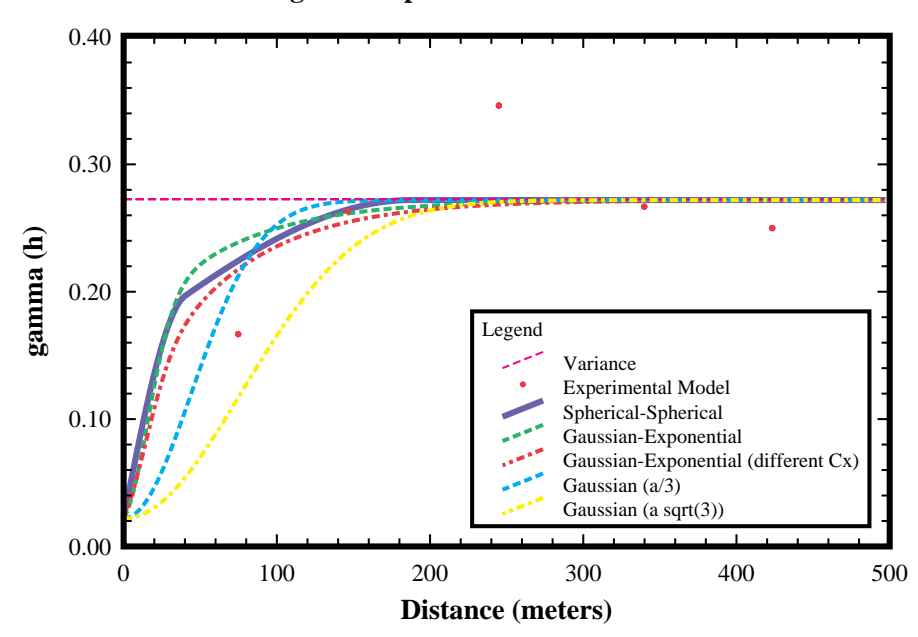


FIGURE 3-5. Semivariogram models used for synthetic directional semivariogram data set. Despite the general rule of thumb that the practical Gaussian range to a spherical range (a) is the SQRT(3) multiplied by the range (a), the Gaussian (range (a) x SQRT(3)) model, because it mimicked the general nature of the other models more closely.

peaks at (100,300: in red), the valley depressions near (425, 210: in blue), and the slope transition at (70, 130). Although Figure 3.3b, and Figures 3.6a through 3.6c appear similar to each other, the mean absolute differences are as much as 7%, and differences between individual cells are up to 37% (Figures 3.7a, 3.7c, and 3.8), when compared to the kriged mapped using anisotropy factors (Figure 3.3b). These scenarios demonstrate how the use of directional semivariogram model descriptions impacts the resulting maps, relative to a scenario which utilizes a compromise semivariogram model with anisotropy factors.

3.5.2.2: Rocky Mountain Arsenal Demonstration Data Set

To demonstrate the effectiveness, and some of the difficulties, of directional kriging, a data set of bedrock surface elevations (actually residuals from a second-order trend-surface) from the Rocky Mountain Arsenal (RMA), Commerce City, Colorado is used. With this data set, use of correct directional semivariogram models reduced the average estimation variance over the map area, even though an artificially large nugget was used. Because of problems with the Gaussian

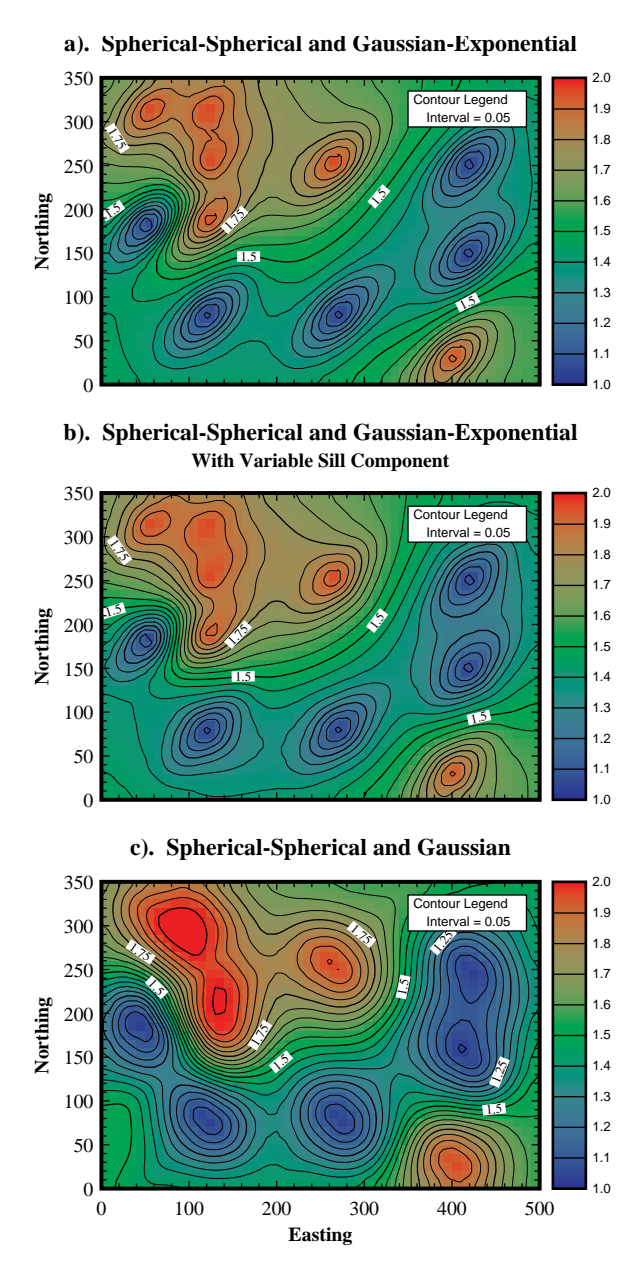
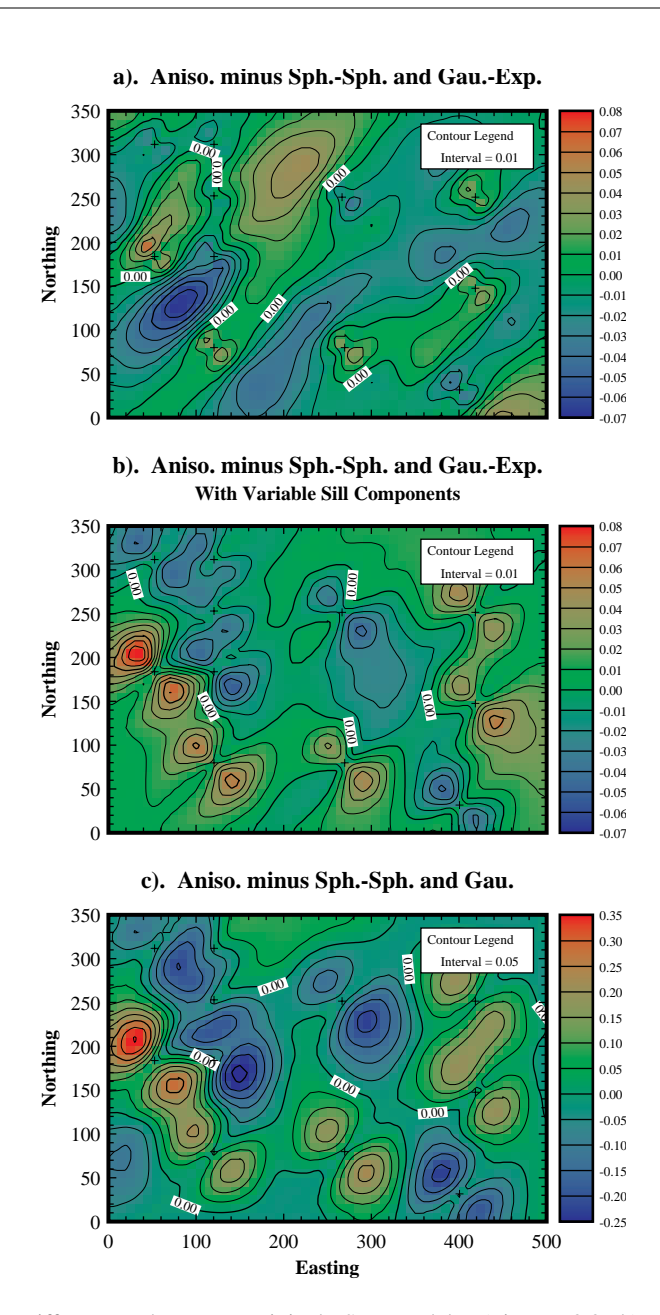


FIGURE 3-6. Results of directional semivariogram models using different assumptions about major and minor semivariogram models.



a). Spherical-Spherical and 20 Gaussian-Exponential Mean = |Difference| = 1.55 | Minimum = -6.74 10 Maximum = 6.22 Frequency (%) b). Spherical-Spherical and 20 Gaussian-Exponential Mean = 0.394 With Variable Sills n |Difference| = 1.52 Minimum = -5.02 Maximum = 8.55 c). Spherical-Spherical and 20 Gaussian rencel = 7.3910 -25 5 -20 -15 -10 -5 0 10 15 20 25 30 35 Percentage Difference

Anisotropic Factor - Directional Models

FIGURE 3-8. Distribution of differences between original SK models (Figure 3.3a-b), and directional semivariogram models (Figures 3.6a-c).

semivariogram model, the nugget term was increased by 260% to stabilize the kriging matrix (Gaussian models can cause singular matrix problems with small nuggets (Ababou, et al., 1994; Posa, 1989)).

3.5.2.2.1: Background

Johnson (1995) had trouble evaluating this site due to constraint related to the semivariogram model definition. She recognized directional differences in spatial statistics, but anisotropy factors would not allow her to model them correctly. As a result, Johnson compromised with a two-nested spherical model. It is important that the RMA be modeled accurately, because, summarizing Johnson (1995), there are many serious environmental concerns:

The RMA was established in 1942 for the production of chemical and incendiary munitions. From 1947 to 1982, herbicides and pesticides were also produced (Environmental Science and Engineering, 1987). During this time chemical agents, such as levinstein mustard (H), phosgene, napalm, isopropylmethyl fluorophosphonate (Sarin or GB), and dichlorodiphenyltrichloroethane (DDT) were produced (Harding Lawson Associates, 1992). Problems arose at the site because liquid wastes were disposed of in lined and unlined evaporation basins, and waste was initially held in settling ponds or transported by sewer or drainage ditch to the basin (Kuznear and Trautmann, 1980). By the 1950's the effects of ground water contamination were noted; there was high waterfowl mortality and extreme crop loss (Harding, Lawson, et al., 1992). By 1974,

disopropylmethylphosphonate (DIMP) and dicyclopentadiene (DCPD) contamination was detected off site (Environmental Science and Engineering, 1987).

Johnson (1995) investigated potential transport routes for contaminants from the RMA. To accomplish this, Johnson (1995) identified and simulated (using conditional indicator simulation) paleo-river channels, coarse and fine sediment distribution, and the ground water surface. The paleo-river channels are of interest because they provide potential pathways for ground water and contaminant movement. To identify these paleo-river channels Johnson (1995) simulated the bedrock surface using boring data from 842 wells. This bedrock surface was identified as an ancient erosional surface which dips slightly to the Northwest towards the Platte River (Harding, et al., 1992).

In Johnson's (1995) work, the regional dip was removed from the bedrock data using a secondorder trend-surface. Using the residual data, Johnson performed semivariogram analyses and conditional simulation. A problem arose during the semivariogram analysis; the experimental semivariograms in the minor and major search directions couldn't be modeled well using a single model semivariogram with anisotropy factors. As a result, compromises were made in selecting semivariogram models (Figure 3.9a) with the hope that, by honoring the short lag data, errors would be acceptably small.

3.5.2.2.2: Directional Semivariogram Kriging

The directional semivariogram kriging technique was to used separate the directional components in semivariogram models. The full series of simulations presented by Johnson (1995) is not repeated here, but the new estimates of the bedrock surface honor the spatial distribution of the data better than the estimates made by Johnson (1995). This is accomplished by using simple kriging and evaluating the estimation variance. The estimation variance is a function of the data locations, and the differences between ordinary kriging and indicator kriging, do not effect the estimation variance. It is important to note that the estimation variance only provides a comparison of alternative data configurations; it is independent of the data values (Deutsch and Journel, 1992).

Four semivariogram models were evaluated: (I) one is similar to Johnson's (1995) two-nested spherical-spherical model with anisotropy factors, but an improved model with a lower mean square error (MSE) is used (Figure 3.9a); (II) another is an accurate directional spherical-spherical / Gaussian model (Figure 3.9b); (III) a second directional model based on II, but with a much larger nugget to accommodate difficulties with the Gaussian model is used (Figure 3.9c), and finally (IV) another two-nested spherical-spherical model with anisotropy factors, but an appropriate nugget is used (Figure 3.9d). The semivariogram models are summarized in Table 3.1.

Model I fits the major-axis (East-West) well, but its spherical-spherical structure is not able to represent the inflection in the early portion of the minor axis (North-South) experimental semivariogram. This model assumes a zero nugget. When this model is used with Simple Kriging on the site data (Figure 3.10a), using a 50 by 50, two-dimensional grid, the smallest estimation variance results of all the semivariogram models are obtained. The kriged surface and estimation variance are shown in Figures 3.10b-c. It is thought that this model underrates the estimation

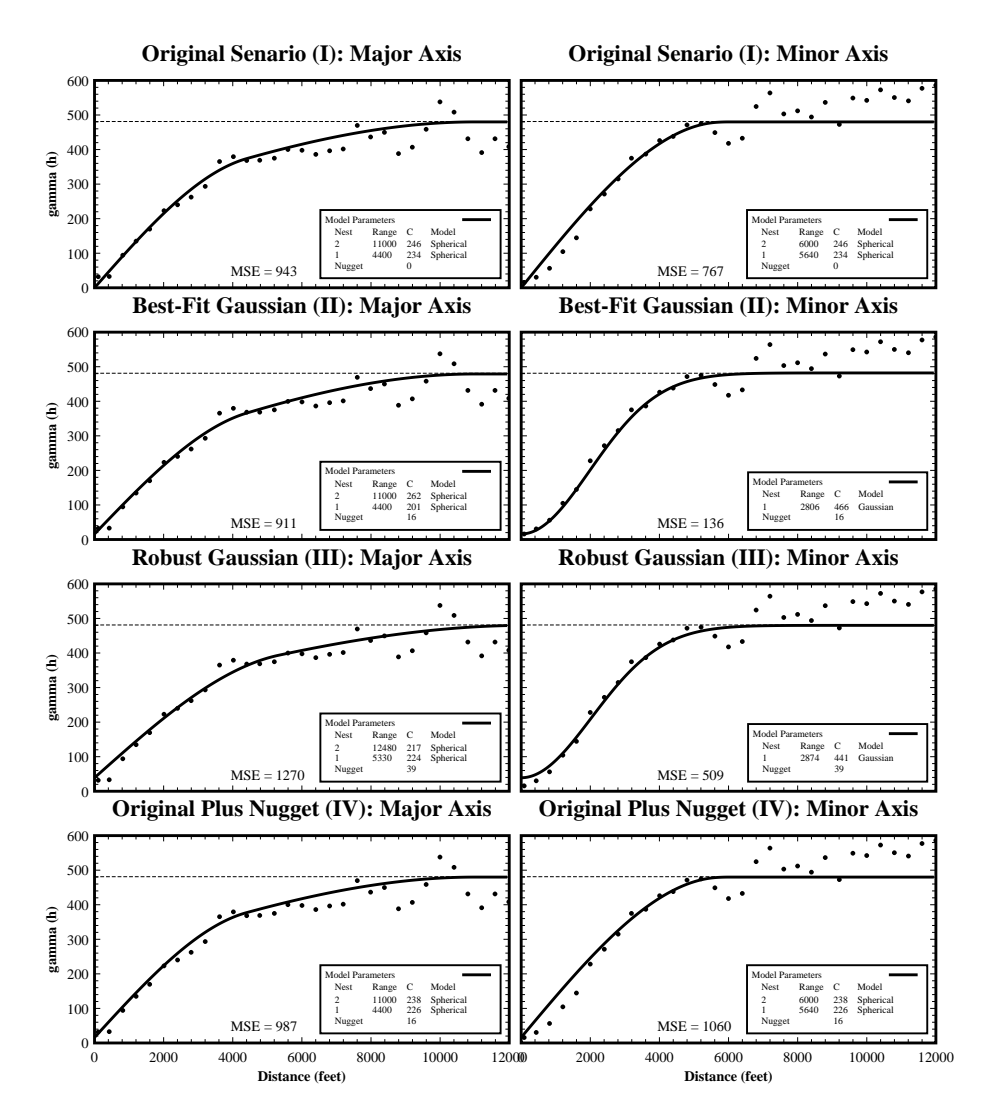


FIGURE 3-9. Experimental and model semivariograms for RMA bedrock residuals (2nd order trend removed): a) anisotropy factor model optimized to minimize MSE based on Johnson (1995), b) optimized minor-axis fit with Gaussian model (note MSE reduced by 82%), c) minor-axis Gaussian model fit with elevated nugget to reduce kriging matrix instability, d) anisotropy factor model optimized to minimize MSE, but also honor nugget defined in b).

variance due to the zero nugget. It is clear that the nugget has a $\gamma(h)$ value of approximately 16 (Figure 3.10b). This incorrect assumption is corrected with model IV.

Model II (Figure 3.9) has the best fit of the four models evaluated, based on MSE measurements of the experimental semivariograms. The fit is particularly good for the minor axis. The MSE for this

Model	Axis	Model Tyoe	Range	Sill	Nugget	Y-Aniso	MSE
I	X/Y	Spherical	4400	234	0	1.833	943/767
		Spherical	11000	246		0.780	
II	X	Spherical	4400	201	16	NA	911
		Spherical	11000	262		NA	
	Y	Gaussian	2806	466	16	NA	136
III	X	Spherical	5330	224	39	NA	1270
		Spherical	12480	217		NA	
	Y	Gaussian	2874	441		NA	509
IV	X/Y	Spherical	4400	226	39	1.833	987/1060
		Spherical	11000	238	16	0.780	

TABLE 3.1. Alternative semivariogram models for RMA residual bedrock surface. Range, sill, and nugget terms are in feet.

axis model is only 12% to 25% of all the other models evaluated. From this model, it was concluded that the nugget has a $\gamma(h)$ value of 16.0. Due to theoretical problems with Gaussian models and the small nugget (less than 10% of the variance) associated with these data, this model has no acceptable solution. Many individual grid cell kriging matrices are singular, or have huge kriging weights (weights greater than ± 1.05 were considered unacceptable; weights greater than ± 200 were found). Regrettably, this behavior is inherent with the Gaussian model, but increasing the nugget increases the stability of every matrix solution (Ababou, et al., 1994; Posa, 1989).

Model III (Figure 3.9c) was developed in an attempt to stabilize the solution, without completely compromising the model results, the nugget was increased until there are no singular matrices or individual kriging weights greater than 1.05 (this allows for some negative kriging weights). To attain this, the nugget was increased to 39.0 (a 244% increase); this is still only 8% of the data set variance. The kriged bedrock surface and estimation variance are shown in Figure 3.11a-b. The average estimation variance is significantly larger for this model than for model I. The difference between the estimation variances (Model III - Model I) are shown in Figures 3.11c and 3.12a. The estimation variance for model III, on average, is 12.7% larger than the estimation variance for model I, but this is not a reasonable reflection of model quality, because the results of model I do not account for the variance due to the nugget.

Model IV (Figure 3.9c) is a modification of model I and accounts for the nugget (although not exaggerated as is necessary for the Gaussian model (III)). The kriged surface and estimation variances are shown in Figure 3.13a-b. The difference between the estimation variances (Model III - Model IV) are shown in Figures 3.13c and 3.12b. Now that the nugget is included, it is reasonable to compare the results of using the traditional anisotropy factor model, to those obtained by using the directional semivariogram model approach. Even though model III has increased the nugget by 244% to stabilize the Gaussian model, the mean difference in the estimation variance between models III and IV is -5.20%. This implies model III's (the directional models) results are better, or at least less uncertain, than the results from model IV. A Q-Q (quantile-quantile) plot is also shown in Figure 3.14 comparing the original (I) estimated residuals vs. each of the other models. It shows

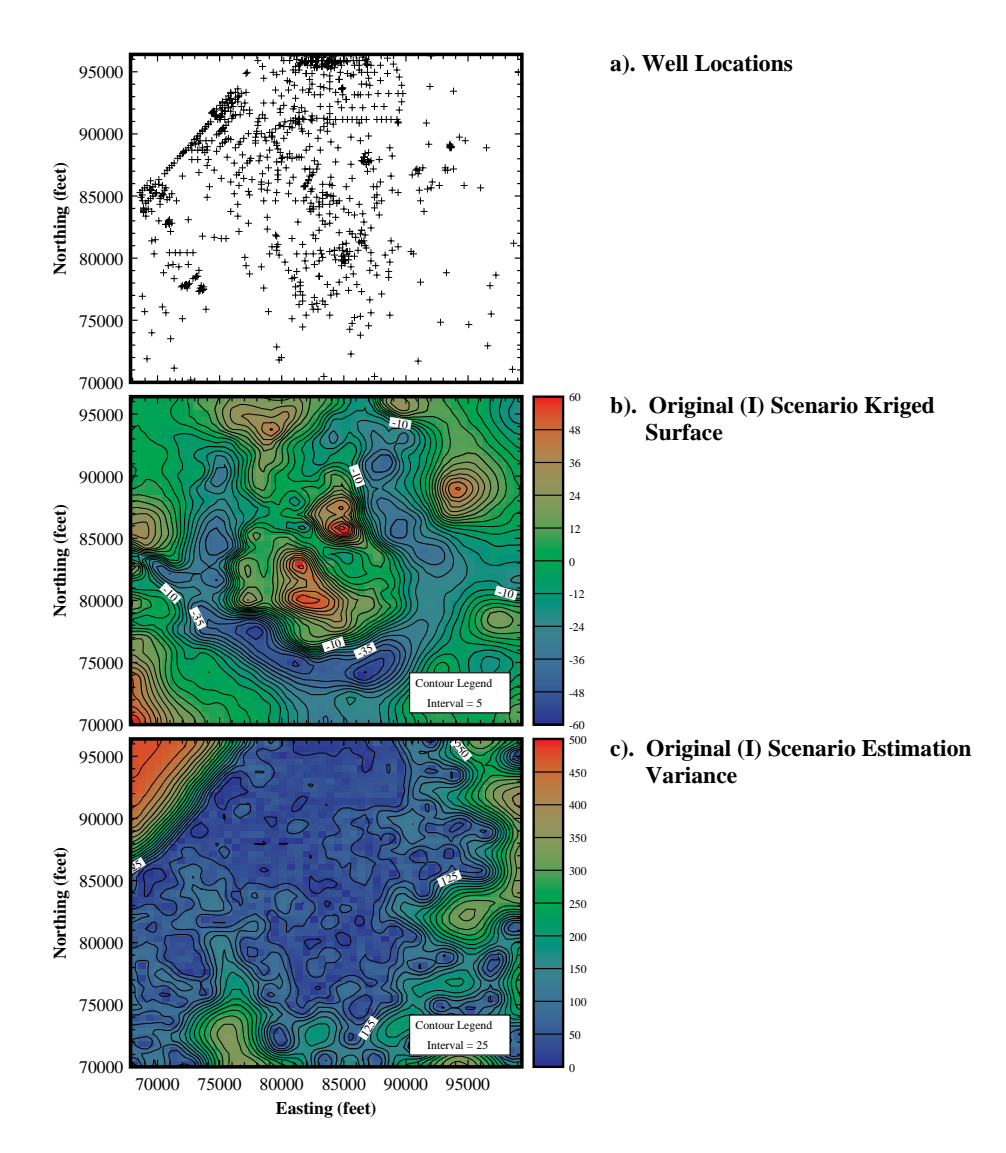


FIGURE 3-10. Location of sample wells at RMA (a), SK map of bedrock elevation residuals (b), and estimation variance using an anisotropy factor, spherical-spherical semivariogram model I (c) (Johnson, 1995).

that the results are similar in all models. Each model generates a similar number of sample values in each of 100 quantiles, but by fine tuning the semivariogram models the estimation variance can be reduced without making any dramatic changes in the overall model statistics.

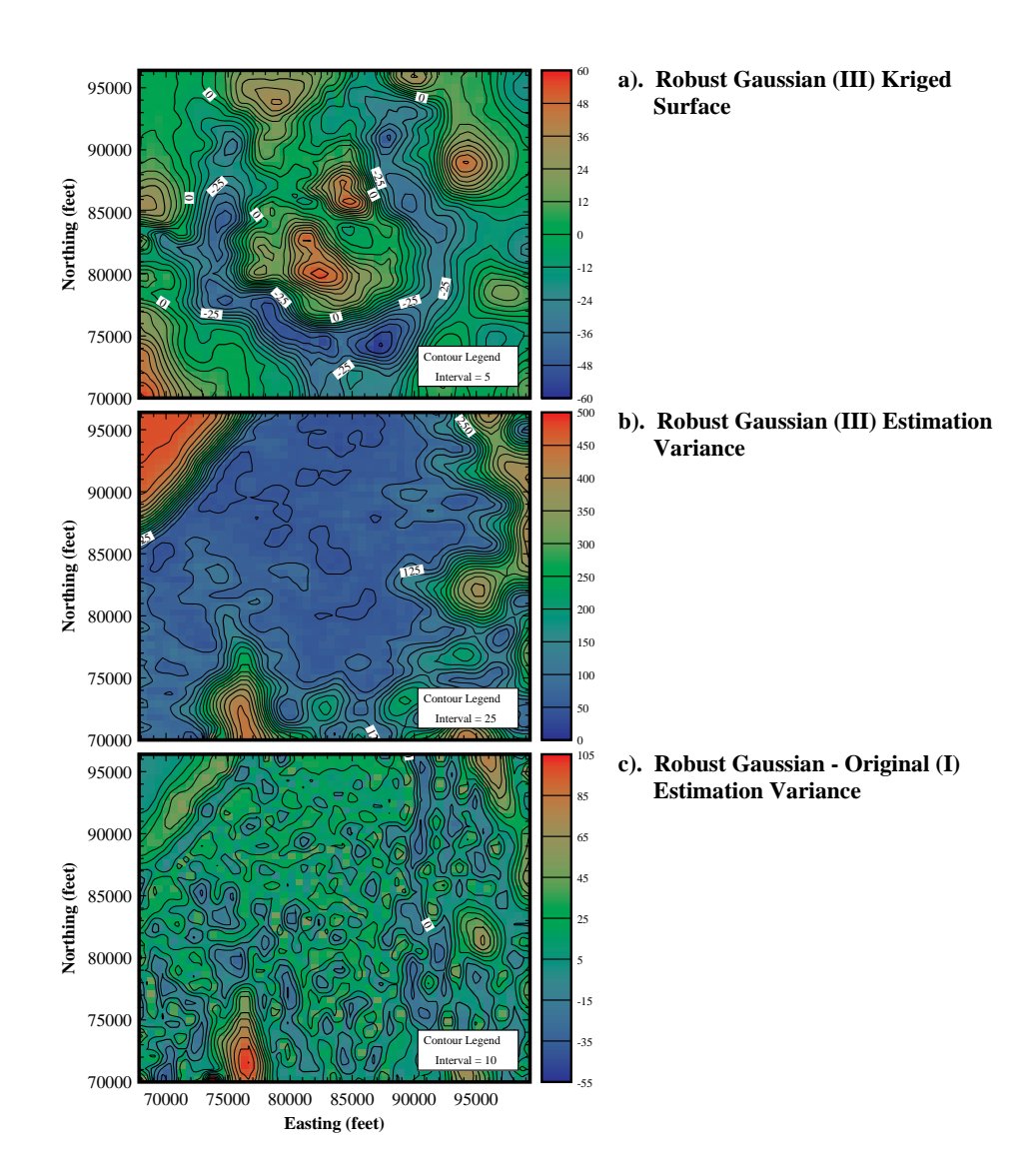


FIGURE 3-11. RMA SK map of bedrock elevation residuals (a), and estimation variance using robust Gaussian factor semivariogram models (b), and difference between robust Gaussian (b) and original (Figure 3.10c) estimation variance maps (c).

In this example, if the nugget is accounted for, the directional semivariograms yield a better result, even when the nugget was artificially exaggerated only for the directional model to prevent problems associated with use of the Gaussian model. In some cases though, unstable models (such as Gaussian) may make the use of directional models undesirable, even when they would, at first, appear justified. As Posa (1989) argues, and his conclusion is supported here, it is sometimes better

a). Gaussian (III) - Original (I) Estimation Variance Mean = 12.7 Median = 10.4 Mean = 10.4 Mean = 10.4 Estimation Difference (ft^2)

b). Gaussian (III) - Original Plus Nugget (IV) Estimation Variance

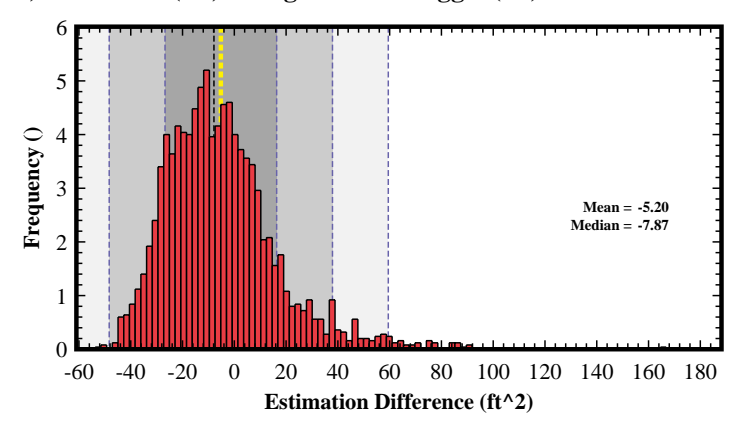


FIGURE 3-12. Distribution of differences between alternative estimation variance maps: (a) the difference between the robust Gaussian (III) and the anisotropy factor, spherical-spherical semivariogram model (I); (b) the difference between the robust Gaussian (III) and the anisotropy factor, spherical-spherical semivariogram model with nugget (I). The positive, average difference in (a) indicates the Gaussian model has a higher average estimation variance. The negative, average difference in (b) indicates the Gaussian model has a lower average estimation variance.

to use a semivariogram model which is not as physically correct, but which is numerically more robust (i.e. a spherical model).

The main problem with implementing directional semivariograms, in this case, was related to the instability in the kriging matrix resulting from theoretical problems associated with using a small nugget and a Gaussian semivariogram model. This, however is a general problem for all kriging methods, and should not reflect adversely on the directional semivariogram method.

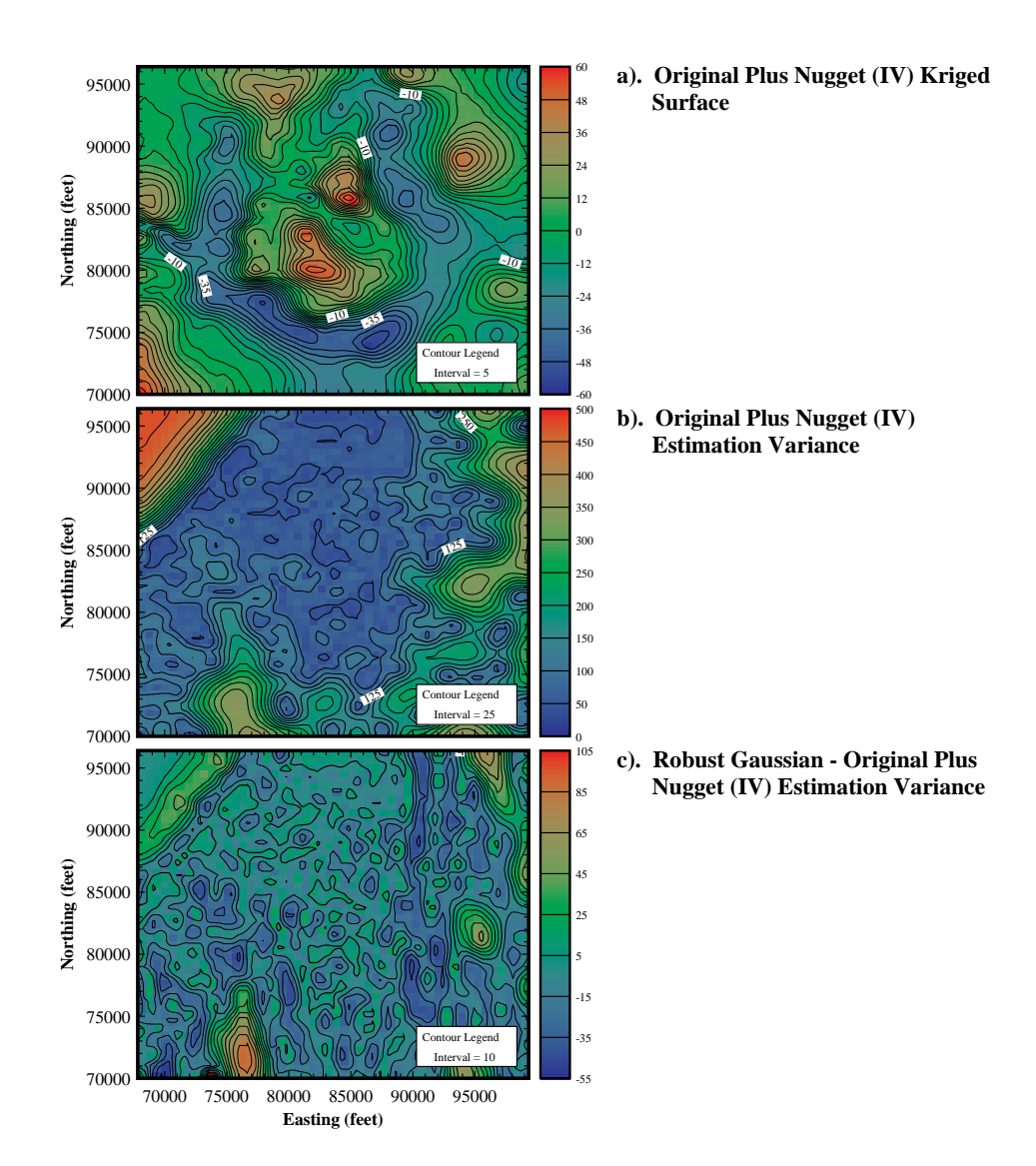


FIGURE 3-13. RMA SK map of bedrock elevation residuals (a), and estimation variance using the anisotropic factor spherical-spherical semivariogram model with a valid nugget (IV) (b), and difference between the robust Gaussian (III) (Figure 3.10c) and estimation variance maps (b).

Change In Estimaed Residuals by ModelQ-Q Plot

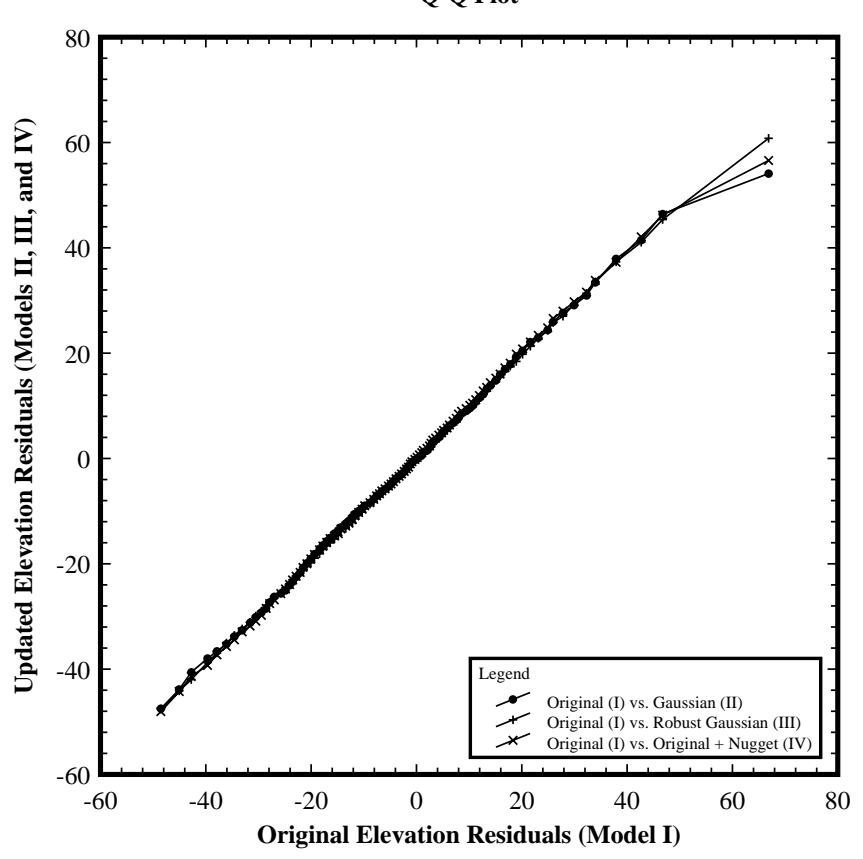


FIGURE 3-14. Q-Q plot of bedrock elevation residuals where the original Spherical model using anisotropy factors (I) is compared versus 1) the original Gaussian model (II), 2) the robust Gaussian model, and 3) the original Spherical model adjusted with a nugget. The plot suggests that the general nature of all the models are similar.

3.6: Conclusions

This chapter demonstrates that better definition of the experimental semivariogram, yields results which better honor the spatial statistics of the sample data. This is illustrated by reduced estimation variance when factors other than model definition are removed. This is accomplished by defining unique model semivariograms along each of the three principle axes of the semivariogram model ellipsoid. In addition to improving the results, the procedure also makes it easier to model

experimental semivariograms, because one need not compromise when selecting model types and sills for each axis. There is an increase in computational effort which increases total processing time in this study (observed times increased 80% to 200%), but this cost is relatively minor when compared to the total time the modeler spends developing semivariogram models. Overall, use of directional semivariogram modeling requires some additional computational time, but modeler effort is reduced, and most important, a significant increase in accuracy may be attained.